RESEARCH ARTICLE
SPACE PHYSICS: IONOSPHERIC PHYSICS

Earth and Planetary Physics
5: 427–434, 2021
doi: 10.26464/epp2021046

Plasma depletions lasting into daytime during the recovery phase of a geomagnetic storm in May 2017: Analysis and simulation of GPS total electron content observations

Yuichi Otsuka[1]*, Atsuki Shinbori[1], Takuya Sori[1], Takuya Tsugawa[2], Michi Nishioka[2], and Joseph D. Huba[3]

[1]Institute for Space-Earth Environmental Research, Nagoya University, Nagoya, Japan;

[2]National Institute of Information and Communications Technology, Tokyo, Japan;

[3]Syntek Technologies, Fairfax, VA, USA

Key Points:

- Plasma density depletions appearing over Japan near sunrise on 29 May 2017 survived until the afternoon during the recovery phase of a geomagnetic storm.
- The initial enhancement of the TEC at sunrise, followed by a reduction in TEC, could be responsible for the long-lasting persistence of plasma depletions during daytime.
- The plasma density depletion in the topside ionosphere is not filled by the plasma generated by solar EUV photoionization for several hours.

Citation: Otsuka, Y., Shinbori, A., Sori, T., Tsugawa, T., Nishioka, M., and Huba, J. D. (2021). Plasma depletions lasting into daytime during the recovery phase of a geomagnetic storm in May 2017: Analysis and simulation of GPS total electron content observations. *Earth Planet. Phys.*, *5*(5), 427–434. http://doi.org/10.26464/epp2021046

Abstract: This paper reports that plasma density depletions appearing at middle latitudes near sunrise survived until afternoon on 29 May 2017 during the recovery phase of a geomagnetic storm. By analyzing GPS data collected in Japan, we investigate temporal variations in the horizontal two-dimensional distribution of total electron content (TEC) during the geomagnetic storm. The SYM-*H* index reached −142 nT around 08 UT on 28 May 2017. TEC depletions extending up to approximately 38°N along the meridional direction appeared over Japan around 05 LT (LT = UT + 9 hours) on 29 May 2017, when TEC rapidly increased at sunrise due to the solar extreme ultraviolet (EUV) radiation. The TEC depletions appeared sequentially over Japan for approximately 8 hours in sunlit conditions. At 06 LT on 29 May, when the plasma depletions first appeared over Japan, the background TEC was enhanced to approximately 17 TECU, and then decreased to approximately 80% of the TEC typical of magnetically quiet conditions. We conclude that this temporal variation of background plasma density in the ionosphere was responsible for the persistence of these plasma depletions for so long in daytime. By using the Naval Research Laboratory: Sami2 is Another Model of the Ionosphere (SAMI2), we have evaluated how plasma production and ambipolar diffusion along the magnetic field may affect the rate of plasma depletion disappearance. Simulation shows that the plasma density increases at the time of plasma depletion appearance; subsequent decreases in the plasma density appear to be responsible for the long-lasting persistence of plasma depletions during daytime. The plasma density depletion in the top side ionosphere is not filled by the plasma generated by the solar EUV productions because plasma production occurs mainly at the bottom side of the ionosphere.

Keywords: plasma bubble; GPS; ionosphere; ionospheric irregularity; SAMI2

1. Introduction

A plasma bubble is a localized depletion of plasma density in the ionosphere. Plasma bubbles are generated at the magnetic equator through the Rayleigh–Taylor instability (e.g., Kelley, 2009) and extend to higher altitudes and latitudes, with structures elongating along the magnetic field lines (e.g., Otsuka et al., 2002a). For the generation of a plasma bubble, eastward electric fields at the magnetic equator play an important role. The eastward electric fields are observed to increase at the evening terminator, before the zonal electric field becomes westward. This phenomenon is called pre-reversal enhancement (PRE). During magnetically quiet conditions, PRE mainly controls plasma bubble occurrence. Most plasma bubbles are observed to be generated at the evening terminator, to survive during nighttime, and to disappear after sunrise, presumably due to plasma production caused by the resumption of solar EUV radiation (e.g., Watanabe and Oya, 1986).

Occasionally, post-sunrise plasma depletions and/or irregularities associated with the plasma bubbles have been observed — by radar (e.g., Chau and Woodman, 2001; Fukao et al., 2003) and by

Correspondence to: Y. Otsuka, otsuka@isee.nagoya-u.ac.jp
Received 07 MAY 2021; Accepted 09 AUG 2021.
Accepted article online 23 AUG 2021.

satellite *in-situ* measurements (e.g., Huang CS et al., 2013). Field Aligned Irregularities (FAIs), which could be generated in plasma bubbles, were observed at 05:00–07:00 LT with 47-MHz radar at Kototabang, Indonesia during a magnetic storm (Fukao et al., 2003). Oya et al. (1986) and Watanabe and Oya (1986) analyzed *in-situ* measurements of the plasma density on the Hinotori satellite, which orbits with an inclination of 31° at a nearly constant altitude of 650 km; they reported statistical regularities in the occurrence of plasma density depletion, noting that the depletions occur quasi-periodically even in the morning hours under sunlit conditions. Their work indicated that plasma bubbles at the topside ionosphere can survive even in sunlit circumstances.

During magnetic storms, plasma bubbles can be generated as late as midnight and/or near sunrise. Huang CS et al. (2013) reported that *in-situ* measurements made above 800 km altitude on the Communication/Navigation Outage Forecasting System (C/NOFS) detected plasma depletions generated post-midnight that lasted until afternoon (14–15 LT) on 1 November 2011, and plasma depletions generated at dawn that lasted until 11 LT on 12 April 2011. They suggested that these plasma depletions were plasma bubbles generated by eastward electric fields associated with magnetic storms. They also suggested that the plasma production rate at the topside ionosphere was not enough to fill such plasma depletions, explaining why they can sometimes persist so long into daytime. By using GPS data in Japan, Li JH et al. (2012) reported plasma density irregularities during the recovery phase of a magnetic storm on 19 March 2001. They found that the irregularities appeared at low and middle latitudes (23°N–45°N) approximately 1 hour before sunrise and survived until about 1.5 hours after sunrise at middle latitudes and more than 4 hours after sunrise at low latitudes. They suggested that low plasma density during daytime, caused by an intense negative storm, might have contributed to the plasma depletion that persisted unusually long into daytime.

In this study, total electron content (TEC) data obtained from the GPS receiver network in Japan is analyzed. We find that TEC depletions appeared at dawn during the recovery phase of a magnetic storm on 27–29 May 2017. The plasma depletions lasted until around 13 LT. It has been suggested that the observed TEC depletions at mid-latitudes may be related to equatorial plasma bubbles (Aa et al., 2019); but this is problematic since it would require bubbles to rise rapidly to very high altitudes (> 2,400 km). Therefore, in this paper we do not refer to the observed TEC depletion as a plasma bubble. We focus on mechanisms that could account for long-lasting TEC depletion during daytime. By carrying out one-dimensional numerical simulations using the SAMI2 model, we have identified a possible mechanism for long-lasting daytime plasma density depletions in the F region.

2. Observations

From carrier phase delays and group delays (C/A and/or P-code pseudoranges) of dual frequency GPS signals (1.57542 GHz and 1.22760 GHz), total electron content (TEC) along a ray path between a GPS satellite and receiver can be obtained. In Japan, the GNSS Earth Observation Network System (GEONET), which as of 2020 consists of approximately 1,300 dual-frequency GPS receivers, has been operated by the Geospatial Information Authority of Japan. TEC is calculated from GEONET GPS data with a time resolution of 30 seconds by using the carrier phase and pseudorange data at the dual frequencies. TEC data obtained from the carrier phase are accurate, but the phase measurement includes ambiguity due to unknown initialization constants. Correction of this phase ambiguity is carried out by use of TEC data obtained from the corresponding pseudorange. The inter-frequency biases included in the TEC data obtained from the above procedure are subtracted, to obtain absolute TEC, by using a method of Otsuka et al. (2002b).

We have analyzed the detrended TEC obtained by subtracting 1-hour running averages (averaged over ±30 minutes centered on the corresponding data) from the original TEC time series for each pair of satellites and receivers (e.g., Saito et al., 1998). ROTI (Rate Of TEC change Index) is widely used to detect plasma density irregularities in the F region (e.g., Pi X et al., 1997; Nishioka et al., 2008). ROTI is a standard deviation of ROT (Rate Of TEC change) in 5 minutes. ROT is obtained from the differential of TEC at 30-second intervals and is represented as the magnitude of TEC change in each minute. For the detrended TEC and ROTI, their slant component is converted to vertical by multiplying a slant factor defined as τ_0/τ_1, where τ_1 is the length of the ray path between 250 and 450 km altitudes and τ_0 is the thickness of the ionosphere (200 km) for the zenith path. According to the method of Saito et al. (1998), in order to distinguish temporal and spatial variations of TEC, the detrended TEC and ROTI with the satellite elevation angle larger than 35° are mapped onto an iono-

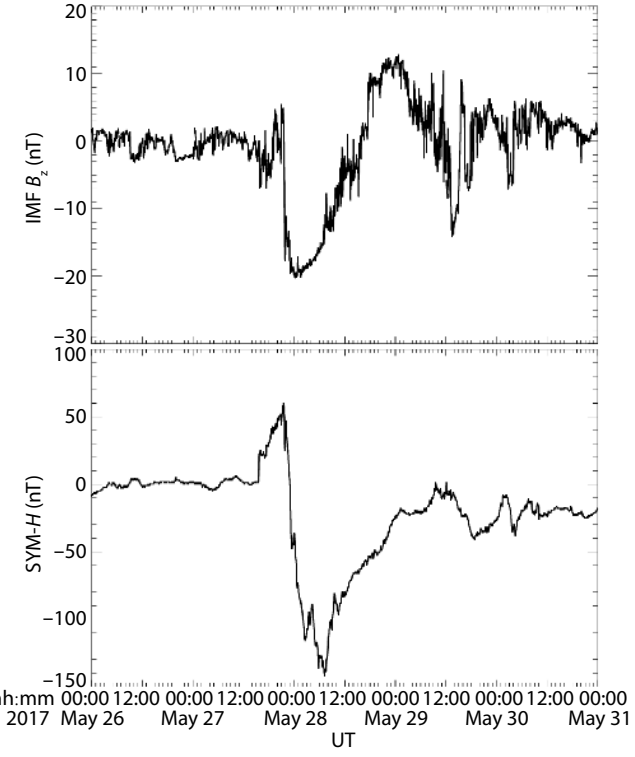

Figure 1. Temporal variation of northward component of interplanetary magnetic field (IMF-B_z) and SYM-H index during a period of 26–30 May, 2017.

spheric shell at a 300 km altitude in the geographical coordinates with a horizontal cell of 0.15° × 0.15° in latitude and longitude.

A corona mass ejection (CME) launched on May 27 2017 triggered a magnetic storm on 27 May 2017 (Liu L et al., 2020). Figure 1 shows temporal variations of the northward component of the Interplanetary Magnetic Field (IMF-B_z) and the SYM-*H* index during a period of 26–30 May 2017. IMF-B_z becomes southward suddenly around 22 UT on 27 May 2017, keeps southward for approximately 20 hours, and turns northward around 16 UT on 28 May. A storm sudden commencement (SSC) occurred around 15:30 UT on 27 May 2017. The SYM-*H* index reached a minimum of −142 nT around 08 UT on May 28, 2017.

Figure 2 shows a time series of the detrended TEC map over Japan between 04:00 and 14:00 LT (UT + 9 hours) on May 29, 2017. Several depleted TEC regions extending in the meridional direction appeared at 05 LT. In the figure, each arrow represents the location of TEC depletions extending in the meridional direction with magnitude exceeding 0.2 TECU. Animation of the detrended TEC map is shown in S1. The plasma depletions moved westward. Magnitude of the TEC depletion decreased with time. At 13 LT, the TEC depletion has a magnitude of approximately 0.2 TECU. At 14 LT, the TEC depletion cannot be seen, indicating that the plasma depletions disappeared.

Figure 3 shows a time series of the ROTI map over Japan between 04 and 09 LT on 29 May 2017. ROTI exceeding 0.2 TECU/min appears at 05 LT. Comparing with the detrended TEC map shown in Figure 2, the high ROTI regions are found to coincide with the TEC depletions, indicating that the ROTI data have captured occurrences of ionospheric plasma density irregularities. However, the ROTI decreases with time, and disappears after 08 LT, whereas the TEC depletion can be seen until 13 LT.

Figure 4 shows local time variation of vertical TEC, averaged over the area of 34°N–36°N and 134°E–136°E in Japan on 29 May 2017. The black curve in the figure represents the vertical TEC averaged over three magnetically quiet days (24–26 May 2017), during which the *Kp* index was less than 1^+. TEC on 29 May 2017 started a rapid increase at 02 LT, reached a peak at 06 LT, and then decreased. The sunrise time at an altitude of 150 km was 03:44 LT (dotted line in the figure). Rapid increase in TEC due to the sunrise started around 05 LT. Comparison with the TEC recorded under quiet conditions reveals that, on 29 May 2017, TEC increase occurred earlier than on magnetically quiet days, and that the peak TEC was approximately two times larger than at the same local time under magnetically quiet conditions. The TEC during daytime on 29 May 2017 was approximately 80% of the TEC observed during magnetically quiet conditions.

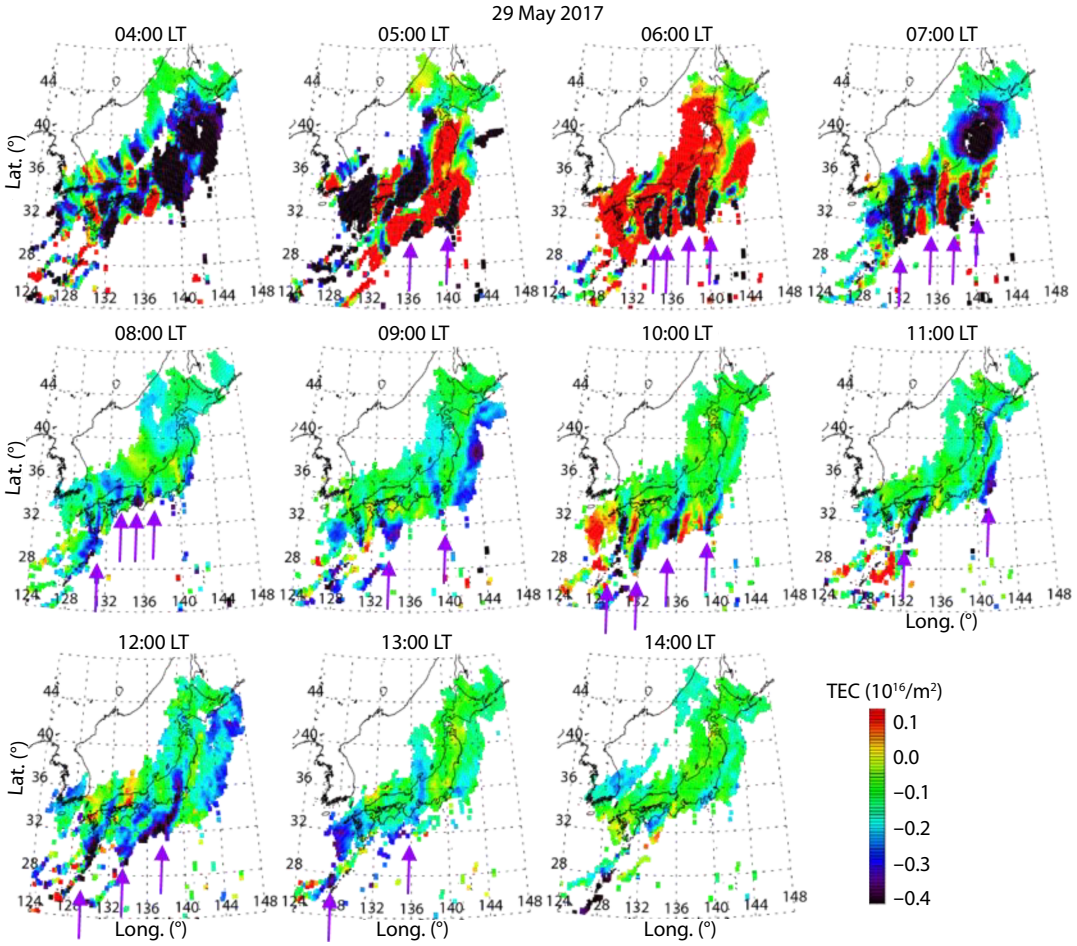

Figure 2. Time sequence of the detrended TEC map over Japan between 04:00 and 14:00 LT (UT + 9 hours) on 29 May 2017. Arrows in the maps point location of TEC depletions.

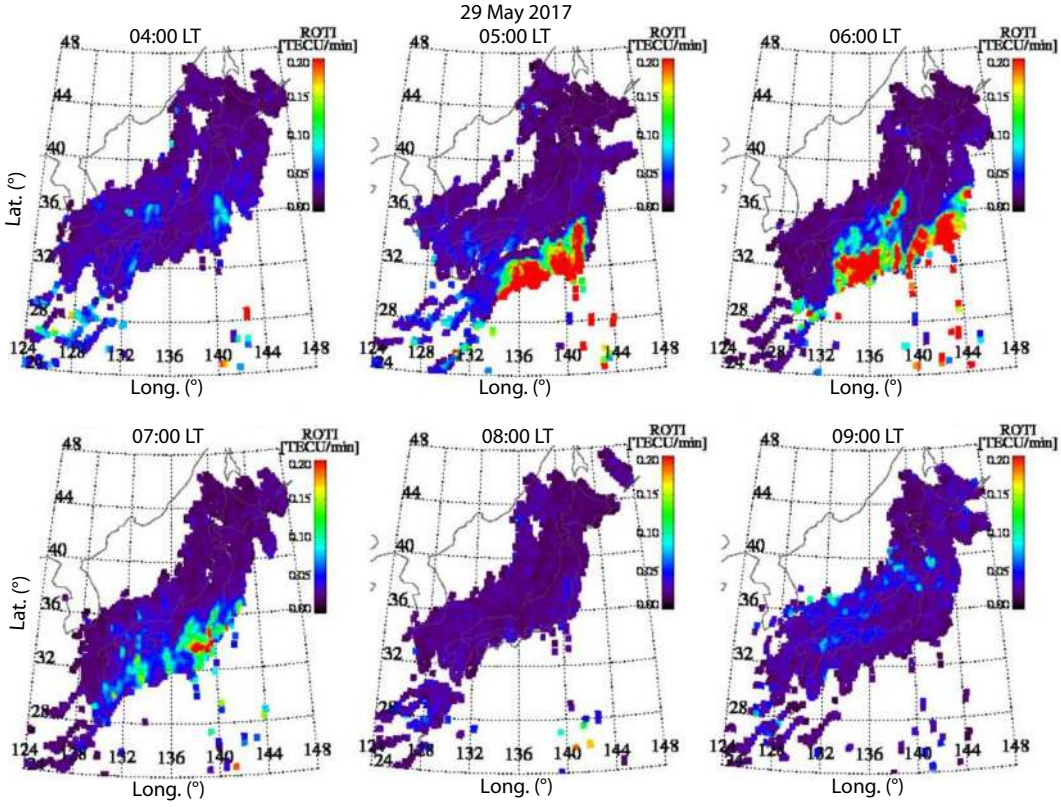

Figure 3. Time sequence of the ROTI map over Japan between 04:00 and 09:00 LT on 29 May 2017.

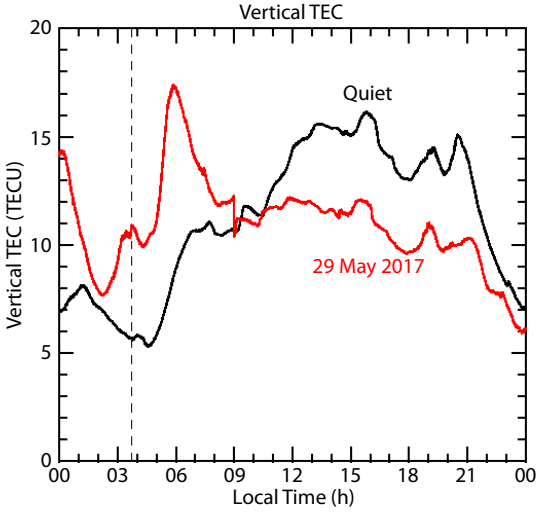

Figure 4. Local time variation of vertical TEC averaged over the area of 34°N–36°N and 134°E–136°E in Japan on 29 May 2017 (red curve). Black curve represents the vertical TEC averaged over three days (24–26 May, 2017) during magnetically quiet days. Vertical broken line represents the time of sunrise at an altitude of 150 km.

3. SAMI2 Simulation

SAMI2 (Another Model of the Ionosphere) is a numerical model in which ion continuity and momentum equations are solved for seven ions (H^+, He^+, N^+, O^+, H_2^+, NO^+, and O_2^+); it also includes temperature equations for H^+, He^+, O^+, and the electrons in an altitude range from 85 km to 20,000 km (Huba et al., 2000). For the neutral atmosphere, we use empirical models NRLMSISE00 (Naval Research Lab Mass Spectrometer and Incoherent Scatter Radar Extended; Picone et al., 2002) and HWM93 (Horizontal Wind Model 1993; Hedin et al., 1996). Also incorporated in the SAMI2 model is EUVAC (EUV model for aeronomical calculations), developed by Richards et al. (1994).

Because plasma diffusion across magnetic field lines is quite slow, as discussed in more detail below in Section 4, using the SAMI2 model in this study has allowed us to evaluate how plasma production and ambipolar diffusion along the magnetic field affects the disappearance of plasma depletions. In particular, we conducted a SAMI2 one-dimensional simulation of the ionosphere connecting a magnetic field line at (35°N, 135°E) in Japan on 29 May 2017, assuming the geophysical condition of Ap = 4, $F_{10.7}$ = 80.0, and 81-days average $F_{10.7}$ = 80. The GPS observations show that the TEC increase at sunrise starts at approximately 05 LT (Figure 4). However, the TEC simulated in SAMI2 increases from 07 LT (not shown). In order to reproduce in the simulation the rapid TEC increase due to solar EUV radiation that was actually observed two hours earlier, we have modified the production rate for the ions in our SAMI2 model, as described below. In SAMI2, the production rate is calculated by the Chapman function, which depends on the solar zenith angle (χ). When χ is between 70° and 100°, the production rate in SAMI2 for this study is calculated using the Chapman function with χ = 70°. When χ varies from 110° to 115°, we assume that χ varies from 70° to 90°. The plasma density and TEC simulated by SAMI2 with the above modification is shown in Figure 5. Local time and altitude cross-section of plasma density is shown in Figure 5a. Local time variation of TEC,

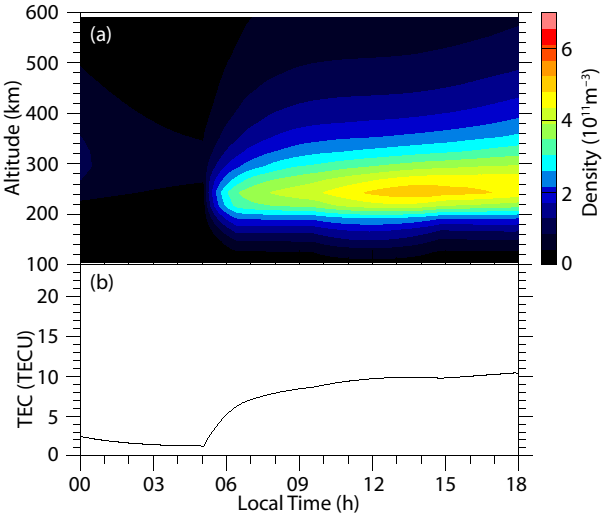

Figure 5. SAMI-2 simulation of the ionospheric plasma density along a magnetic field line over Japan for 29 May 2017 (Case 1). (a) Local Time and altitude cross-section of the plasma density. (b) Local Time variation of TEC obtained from an integration of the plasma density over an altitude range from 100 to 600 km.

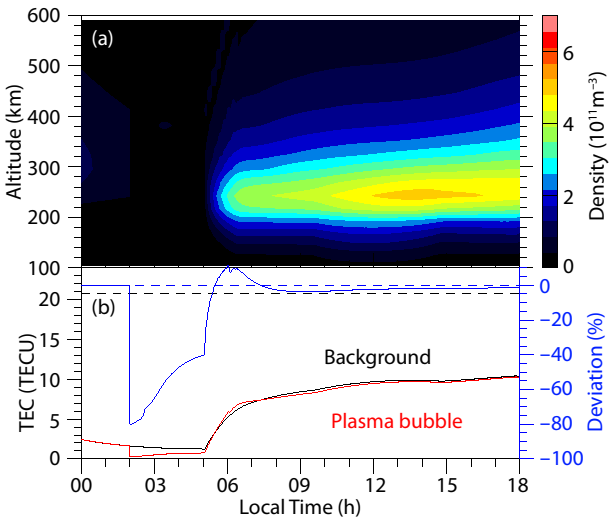

Figure 6. Same as Figure 5 but for Case 1a, in which the plasma density for all altitudes at 02 LT is artificially reduced by 80% from that in Case 1 to simulate a plasma density depletion. Figure 5b shows local time variation of TEC (T_p) obtained from an integration of the plasma density over an altitude range from 100 to 600 km (shown by red). A black curve represents TEC (T_b) obtained for Case 1 as background of the plasma density depletion. A blue curve represents ratio of TEC depletion to the background in percentage, defined as $(T_p–T_b)/T_b$.

which is an integration of the plasma density from 200 km to 600 km in altitude, is shown in Figure 5b. The plasma density rapidly increases after 05 LT, now matching the observed TEC. TEC increases up to approximately 10 TECU.

To simulate plasma density depletion, we have artificially reduceed the plasma density by 80% at a certain time in the simulation, and continued the simulation to investigate temporal variation of the plasma density in plasma depletion. Plasma density in the background (outside of the plasma depletions) is provided by running the simulation without the artificial reduction of plasma density. In this study, we investigate (1) how fast the plasma depletion observed during nighttime disappears after sunrise, (2) whether plasma depletions that first appear after the sunrise plasma density increase can survive for significant amounts of time during daytime, and (3) whether the TEC enhancement after sunrise contributes to prolonging the lifetime of a plasma depletion. Table 1 shows a summary of the cases simulated by SAMI2 in this study. Cases 1 and 2 are used for the background plasma density; Cases 1a, 1b, and 2a are used for the plasma density in the plasma depletions.

For Case 1a, we investigate how fast nighttime plasma depletion disappears after sunrise. The plasma density along the magnetic field is reduced by 80% from the original data at 02 LT to simulate an instance of nighttime plasma depletion. The simulated plasma density, shown in Figure 6a, represents the plasma density in the plasma depletion as a function of time and altitude. TEC (T_p) in the plasma depletion is shown by a red curve in Figure 6b. As TEC (T_p) at the outside of plasma depletion, TEC simulated in Case 1 (shown in Figure 5) is shown by a black curve. Ratio of TEC depletion to that in the outside, defined as $(T_p - T_b)/T_b$, is shown by a blue curve in Figure 6b. In the simulation, the plasma density depletion is maintained until approximately 05:30 LT, but then the plasma depletion disappears rapidly by 06 LT, when the plasma density increases rapidly at the sunrise, indicating that nighttime plasma depletions disappear soon after the sunrise plasma density increase.

Table 1. Simulation cases.

Case 1	Case for May 28, 2017
Case 1a	Case 1 with plasma density reduction by 90% at 4 LT
Case 1b	Case 1 with plasma density reduction by 90% at 9 LT
Case 2	Case 1 with increase of O density
Case 2a	Case 2 with plasma density reduction by 90% at 9.5 LT

As Case 2, we have simulated a plasma depletion that appears after sunrise. The results are shown in Figure 7. The plasma density was artificially reduced by 80% for all altitudes at 06 :15 LT. The background TEC shown in Figure 7b is same as that in Case 1. As shown by the blue curve in Figure 7b, the magnitude of the TEC depletion in the plasma depletion soon decreases, becoming 5% by roughly 11 LT, which is approximately 5 hours after the plasma depletion's appearance. This result indicates that a plasma depletion appearing after sunrise will disappear in approximately 5 hours.

The GPS–TEC map shows that plasma depletions can survive until 13 LT. This discrepancy could be attributed to the difference in temporal variation of the background plasma density. On 29 May 2017, the observed TEC increased at sunrise, reaching a peak around 06 LT. When the TEC depletions appeared over Japan, TEC was enhanced. To simulate such a condition, we artificially increased the plasma density by modifying the oxygen density, which is proportional to production of the plasma in the ionosphere: we increased oxygen density by a factor of eight for all

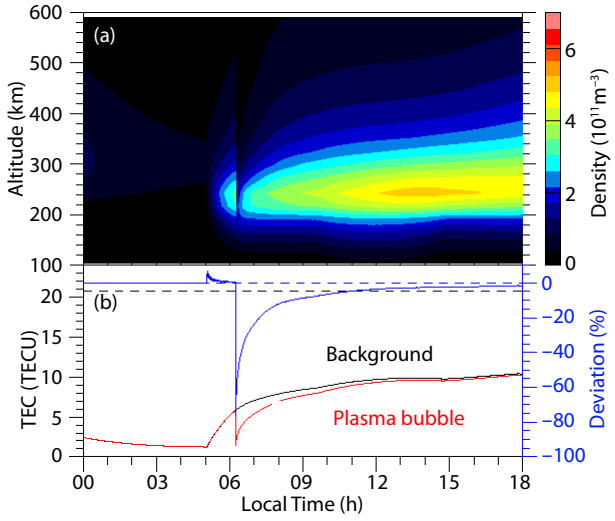

Figure 7. Same as Figure 6 but for Case 1b. The plasma density for all altitudes are artificially reduced by 80% at 08 LT to simulate a plasma density depletion.

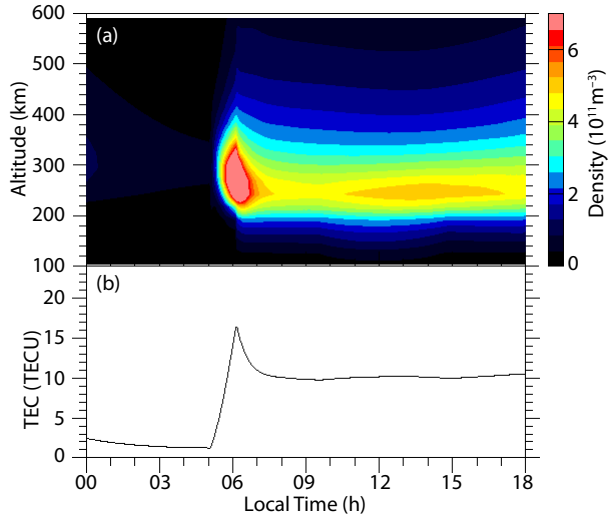

Figure 8. Same as Figure 5 but for Case 2. In the SAMI-2 simulation, the oxygen density is increased by eight times for all altitudes between 05 and 06 LT.

altitudes for one hour between 05 and 06 LT. Local time and altitude cross-section of the plasma density and local time variation of TEC are shown in Figure 8 (Case 2). The resultant TEC reaches its peak value of 16 TECU at 06:15 LT, and then decreases with time. This temporal variation of TEC is similar to the observation shown in Figure 4. In this background condition, we have artificially decreased plasma density for all altitudes by 80% at 06:15 LT to reproduce the plasma depletion appearing when the background plasma density is enhanced (Case 2a). The results are shown in Figure 9: after the plasma density and TEC decrease at 06:15 LT, the magnitude of TEC depletion decreases with time, reaching approximately 5% at around 14 LT, indicating that such plasma depletions can survive approximately 8 hours during daytime. Figure 9a indicates that although the plasma density at altitudes of 200–300 km increases rapidly after the plasma density reduction, the plasma density above 300 km increases only gradually. In order to investigate temporal variation of the plasma density at different altitudes, altitude profiles of the plasma density simulated by SAMI2 for (black) Case 2 and (red) Case 2a are shown in Figure 10. Time above each figure represents the elapsed time from the input of plasma depletion. The simulated plasma density at bottomside of the F layer recovers in 30 minutes. On the other hand, above the F2 peak, the decrease in the plasma density is maintained more than 2.5 hours.

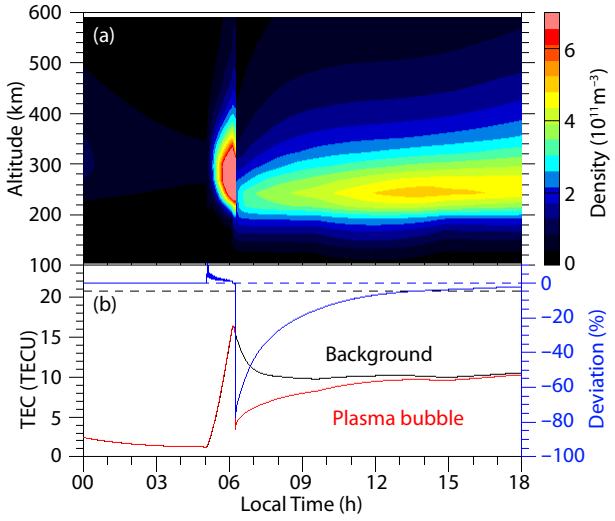

Figure 9. Same as Figure 8 but for Case 2a, in which the plasma density for all altitudes at 06:15 LT are artificially reduced by 80% from that for Case 2.

4. Discussion

Most plasma bubbles are generated at the evening terminator and survive throughout the night. Since ionospheric plasma is not produced during nighttime, the plasma bubble structure decays only due to plasma diffusion in the direction perpendicular to the geomagnetic field lines (Kelley, 2009). The time constant of the diffusion is expressed as $\left(k^2D\right)^{-1}$, where k is the wavenumber of the plasma structure, and D is the diffusion coefficient in the direction perpendicular to the geomagnetic field line. Since D is approximately 1 m/s^2, the time constant for a 1-km scale structure is approximately 8 hours (Kelley, 2009). This explains why plasma bubbles, which have zonal scale sizes of approximately 100 km, can survive during a whole night with minimal decay. The SAMI2 simulations in this study demonstrate that the plasma density depletion disappears immediately after the sunrise, indicating that the plasma produced by solar radiation restores the depleted plasma.

Using the SAMI2 model, we have also simulated a case in which a plasma density depletion appears after sunrise, and found that such a depletion is maintained for a few hour into the sunlit period. However, the life-time of the simulated plasma depletion is shorter than that of the TEC depletion observed by the GPS–TEC over Japan on 29 May 2017. On that day, TEC increased rapidly at sunrise, and reached a peak around 06 LT. The TEC was approximately twice as large as is observed under magnetically quiet conditions. After the TEC enhancement, the TEC decreased to approx-

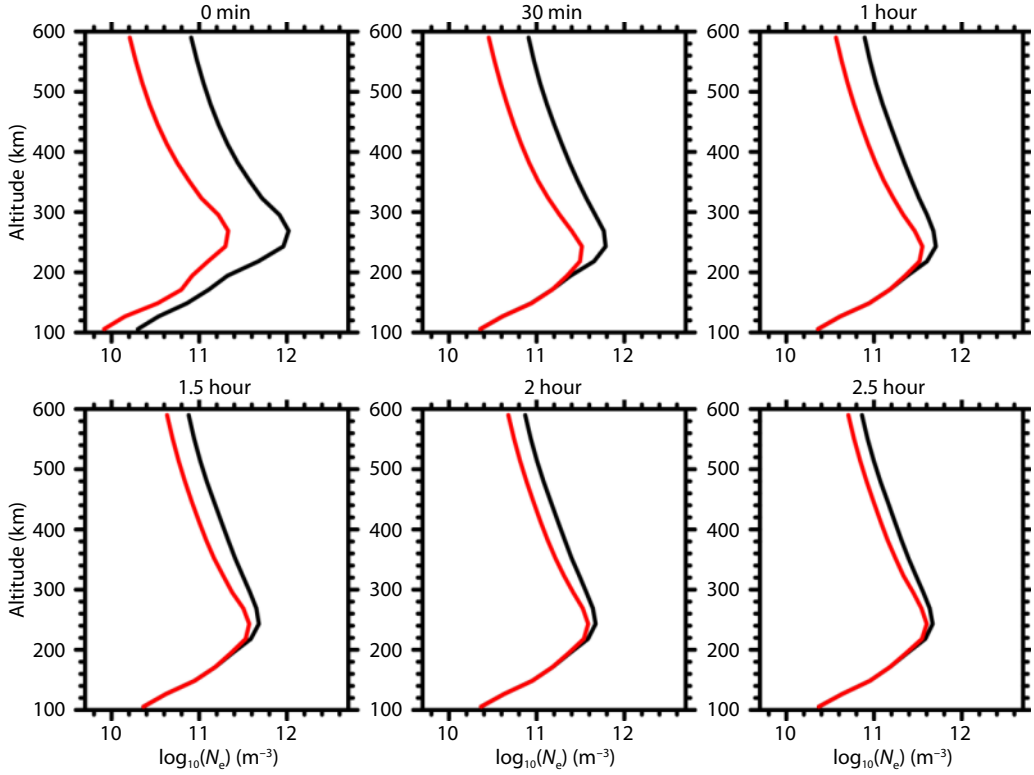

Figure 10. Altitude profile of the plasma density simulated by SAMI-2 for (black) Case 2 and (red) Case 2a. Time above each figure represents the elapsed time from the input of plasma density depletion.

imately 80% of the TEC typical during magnetically quiet conditions. This TEC decrease corresponds to a negative storm. Liu L et al. (2020), who have compared TEC data over China with [O]/[N_2] observed with TIMED-GUVI, report that the TEC decrease on 29–30 May 2017 coincided with a decrease in [O]/[N_2]. The negative storm on 29 May 2017 could have been caused by the decrease in [O]/[N_2].

SAMI2 model simulations in this study show that the plasma density enhancement at the time of appearance of such a plasma depletion and the following decrease in plasma density are responsible for such long-lasting daytime plasma depletions. Below the F2 peak altitude, the plasma depletion is filled by the newly produced plasma. On the other hand, above the F2 peak, the plasma production rate is small, and the altitude profile of the plasma density follows ambipolar diffusion, so that the plasma density above the F2 peak is controlled by the plasma density at the F2 peak altitude. Because the plasma density at the F2 peak is lower during daytime than at the time when the plasma depletions appear, the plasma depletion above F2 peak is maintained longer.

The current GPS–TEC observation shows that plasma depletions survived long after sunrise. The plasma depletions discussed here appeared first over Japan around 05 LT, approximately 4 hours after the northward turning of IMF-B_z, at which time an overshielding electric field, which is eastward during nighttime and dawn and westward during daytime and dusk, could have developed (e.g., Fejer et al., 1979). The eastward electric field at dawn could be a driver of the generation of plasma bubbles at the magnetic equator, through the Rayleigh–Taylor instability. During the recovery phase of a magnetic storm, a disturbance dynamo electric field, which is eastward during nighttime and dawn and westward during daytime and dusk, is also developed (e.g., Fejer et al., 1983). Since the direction of such disturbance dynamo electric fields is the same as that of the over-shielding electric field, the additional eastward electric fields generated by the disturbance dynamo also could contribute to the generation of plasma bubbles at the magnetic equator. The eastward electric fields could be responsible for the TEC enhancement at sunrise, through expansion of the equatorial ionization anomaly to middle latitudes. However, it should be noted that further studies are needed to clarify mechanisms for development of plasma depletion to middle latitudes, about which little is currently known (Aa et al., 2019). ROTI enhancement coincided with TEC depletion when TEC depletions appeared around sunrise. Since high ROTI values represent existence of plasma density irregularities, this result indicates that plasma depletions are generated around the sunrise. The ROTI enhancement disappeared earlier than the TEC depletion. ROTI represents existence of the plasma density irregularities with scale size of several tens of kilometers, because the ionospheric pierce points move at approximately 100 m/s (e.g., Nishioka et al., 2008). As described in the first paragraph of this section, it is diffusion perpendicular to the geomagnetic field that causes plasma density irregularities to disappear. Smaller scale irregularities disappear earlier than large-scale irregularities (Basu et al., 1978). On the other hand, plasma density depletions are observed to survive longer — until afternoon. As discussed above, when plasma depletions occur at times of background plasma density enhancement, that enhancement contributes to longer survival into daytime of such a plasma depletion.

5. Conclusions

We have analyzed GPS–TEC data collected in Japan to investigate temporal variations of horizontal two-dimensional distribution of TEC during a geomagnetic storm which exhibited a minimum SYM-*H* index of −142 nT at approximately 08 UT on May 28, 2017. These TEC observations disclosed the following features:

(1) TEC depletions appeared over Japan at 05 LT (LT = UT + 9 hours) on May 29, 2017, when TEC rapidly increased at sunrise due to the solar EUV radiation. The depletions elongated in the meridional direction and extended up to approximately 38°N in the meridional direction. These TEC depletions appeared sequentially over Japan during the daytime, lasting for approximately 8 hours in sunlit conditions.
(2) The background TEC at 06 LT on May 29, when the TEC depletions, appeared was enhanced to approximately 17 TECU and then decreased. These TEC variations are effects of the geomagnetic storm.

The observed TEC depletions may be related to plasma bubbles generated at the magnetic equator around sunrise, although further studies are needed to clarify the mechanisms for development of plasma density depletions to middle latitudes.

In order to disclose the mechanism that would allow such plasma depletions to last for such a long time during daytime, we carried out SAMI2 one-dimensional simulations and investigated effects on plasma depletions of plasma production and ambipolar diffusion along the magnetic field. We report that plasma depletions can persist during daytime when the plasma density increases at the time when a TEC depletion appears and then decreases. When a strong negative storm follows the plasma density enhancement at sunrise, such a sequence could contribute to the appearance of long-lasting plasma density depletions during daytime.

Acknowledgments

The GPS data in Japan were provided by The Geospatial Information Authority of Japan. The GPS–TEC data are archived by the National Institute of Information and Communications Technology, Japan. The SYM-*H* index was obtained from the GSFC/SPDF OMNIWeb (https://omniweb.gsfc.nasa.gov). IMF data were provided by NASA's CDAWeb (https://cdaweb.sci.gsfc.nasa.gov/index/.html). The *Kp* index was provided by the WDC for Geomagnetism, Kyoto (http://wdc.kugi.kyoto-u.ac.jp/wdc/Sec3.html). This work was supported by the Japan Society for the Promotion of Science, KAKENHI Grants, 16H06286 and 20H00197. This research was supported by NASA (NNH17ZDA001N07) and NSF (AGS-1931415) grants (JDH).

References

Aa, E. C., Zou, S. S., Ridley, A., Zhang, S. R., Coster, A. J., Erickson, P. J., Liu, S. Q., and Ren, J. E. (2019). Merging of storm time midlatitude traveling ionospheric disturbances and equatorial plasma bubbles. *Space Wea.*, *17*(2), 285–298. https://doi.org/10.1029/2018SW002101

Basu, S., Basu, S., Aarons, J., McClure, J. P., and Cousins, M. D. (1978). On the coexistence of kilometer- and meter-scale irregularities in the nighttime equatorial *F* region. *J. Geophys. Res.*: *Space Phys.*, *83*(A9), 4219–4226. https://doi.org/10.1029/JA083iA09p04219

Chau, J. L., and Woodman, R. F. (2001). Interferometric and dual beam observations of daytime Spread-*F*-like irregularities over Jicamarca. *Geophys. Res. Lett.*, *28*(18), 3581–3584. https://doi.org/10.1029/2001GL013404

Fejer, B. G., Gonzales, C. A., Farley, D. T., Kelley, M. C., and Woodman, R. F. (1979). Equatorial electric fields during magnetically disturbed conditions 1. The effect of the interplanetary magnetic field. *J. Geophys. Res.*: *Space Phys.*, *84*(A10), 5797–5802. https://doi.org/10.1029/JA084iA10p05797

Fejer, B. G., Larsen, M. F., and Farley, D. T. (1983). Equatorial disturbance dynamo electric fields. *Geophys. Res. Lett.*, *10*(7), 537–540. https://doi.org/10.1029/GL010i007p00537

Fukao, S., Ozawa, Y., Yamamoto, M., and Tsunoda, R. T. (2003). Altitude-extended equatorial spread *F* observed near sunrise terminator over Indonesia. *Geophys. Res. Lett.*, *30*(22), 2137. https://doi.org/10.1029/2003GL018383

Hedin, A. E., Fleming, E. L., Manson, A. H., Schmidlin, F. J., Avery, S. K., Clark, R. R., Franke, S. J., Fraser, G. J., Tsuda, T., Vial, F., and Vincent, R. A. (1996). Empirical wind model for the upper, middle and lower atmosphere. *J. Atmos. Terr. Phys.*, *58*(13), 1421–1447. https://doi.org/10.1016/0021-9169(95)00122-0

Huang, C. S., de La Beaujardiere, O., Roddy, P. A., Hunton, D. E., Ballenthin, J. O., and Hairston, M. R. (2013). Long-lasting daytime equatorial plasma bubbles observed by the C/NOFS satellite. *J. Geophys. Res.*: *Space Phys.*, *118*(5), 2398–2408. https://doi.org/10.1002/jgra.50252

Huba, J. D., Joyce, G., and Fedder, J. A. (2000). Sami2 is Another Model of the Ionosphere (SAMI2): A new low-latitude ionosphere model. *J. Geophys. Res.*: *Space Phys.*, *105*(A10), 23035–23053. https://doi.org/10.1029/2000JA000035

Kelley, M. C. (2009). *The Earth's Ionosphere: Plasma Physics and Electrodynamics, International Geophysics Series, vol. 96* (2nd ed). San Diego, California: Academic Press.

Li, J. H., Ma, G. Y., Maruyama, T., and Li, Z. (2012). Mid-latitude ionospheric irregularities persisting into late morning during the magnetic storm on 19 March 2001. *J. Geophys. Res.*: *Space Phys.*, *117*(A8), A08304. https://doi.org/10.1029/2012JA017626

Liu, L., Zou, S. S., Yao, Y. B., and Aa, E. (2020). Multi-scale ionosphere responses to the May 2017 magnetic storm over the Asian sector. *GPS Solut.*, *24*(1), 26. https://doi.org/10.1007/s10291-019-0940-1

Nishioka, M., Saito, A., and Tsugawa, T. (2008). Occurrence characteristics of plasma bubble derived from global ground-based GPS receiver networks. *J. Geophys. Res.*: *Space Phys.*, *113*(A5), A05301. https://doi.org/10.1029/2007JA012605

Otsuka, Y., Shiokawa, K., Ogawa, T., and Wilkinson, P. (2002a). Geomagnetic conjugate observations of equatorial airglow depletions. *Geophys. Res. Lett.*, *29*(15), 43–1. https://doi.org/10.1029/2002GL015347

Otsuka, Y., Ogawa, T., Saito, A., Tsugawa, T., Fukao, S., and Miyazaki, S. (2002b). A new technique for mapping of total electron content using GPS network in Japan. *Earth Planets Space*, *54*(1), 63–70. https://doi.org/10.1186/BF03352422

Oya, H., Takahashi, T., and Watanabe, S. (1986). Observation of low latitude ionosphere by the impedance probe on board the Hinotori satellite. *J. Geomag. Geoelectr.*, *38*(2), 111–123. https://doi.org/10.5636/jgg.38.111

Pi, X., Mannucci, A. J., Lindqwister, U. J., and Ho, C. M. (1997). Monitoring of global ionospheric irregularities using the worldwide GPS network. *Geophys. Res. Lett.*, *24*(18), 2283–2286. https://doi.org/10.1029/97GL02273

Picone, J. M., Hedin, A. E., Drob, D. P., and Aikin, A. C. (2002). NRLMSISE-00 empirical model of the atmosphere: Statistical comparisons and scientific issues. *J. Geophys. Res.*: *Space Phys.*, *107*(A12), SIA 15-1–SIA 15-16. https://doi.org/10.1029/2002JA009430

Richards, P. G., Fennelly, J. A., and Torr, D. G. (1994). EUVAC: A solar EUV Flux Model for aeronomic calculations. *J. Geophys. Res.*: *Space Phys.*, *99*(A5), 8981–8992. https://doi.org/10.1029/94JA00518

Saito, A., Fukao, S., and Miyazaki, S. (1998). High resolution mapping of TEC perturbations with the GSI GPS network over Japan. *Geophys. Res. Lett.*, *25*(16), 3079–3082. https://doi.org/10.1029/98GL52361

Watanabe, S., and Oya, H. (1986). Occurrence characteristics of low latitude ionosphere irregularities observed by impedance probe on board the Hinotori satellite. *J. Geomag. Geoelectr.*, *38*(2), 125–149. https://doi.org/10.5636/jgg.38.125